Quantized topological Hall effect in skyrmion crystal

Keita Hamamoto,[1] Motohiko Ezawa,[1] and Naoto Nagaosa[1,2]
[1]*Department of Applied Physics, University of Tokyo, 7-3-1 Hongo, Bunkyo-ku, Tokyo 113-8656, Japan*
[2]*RIKEN Center for Emergent Matter Science (CEMS), Wako, Saitama 351-0198, Japan*
(Received 22 April 2015; published 11 September 2015)

We theoretically study the quantized topological Hall effect (QTHE) in skyrmion crystal (SkX) without external magnetic field. The emergent magnetic field in SkX could be gigantic, as much as 4000 T, when its lattice constant is 1 nm. The band structure is not flat but has a finite gap in the low electron-density regime. We also study the conditions to realize the QTHE for the skyrmion size, carrier density, disorder strength, and temperature. Comparing the SkX and the system under the corresponding uniform magnetic field, the former is more fragile against the temperature compared with the latter since the gap is reduced by a factor of 1/5, while they are almost equally robust against the disorder. Therefore, it is expected that the QTHE of the SkX system is realized even with strong disorder at room temperature when the electron density is of the order of 1 per skyrmion.

DOI: 10.1103/PhysRevB.92.115417 PACS number(s): 73.43.Cd, 03.65.Vf, 73.50.−h

I. INTRODUCTION

Magnetic skyrmion is a topological spin texture in ferromagnets [1]. After the early theoretical proposals in magnets [2–4], the study of magnetic skyrmion has grown rapidly since it was discovered experimentally [5–7]. The periodic array of skyrmions, i.e., a skyrmion crystal (SkX), is realized at interfaces [7] or in bulk chiral magnets such as B20 compounds [5,6]. An emergent magnetic field is generated in the background skyrmion spin texture. Namely, a skyrmion has one magnetic flux $\Phi_0 = h/e$ acting on the conduction electrons coupled to it. When the skyrmions form a periodic lattice, i.e., a SkX, the emergent magnetic field reaches $\sim$4000 T *assuming* the uniform averaged flux for the skyrmion size and the lattice constant of SkX of the order of $\sim$1 nm. The effective magnetic field is proportional to λ^{-2}, where λ is the skyrmion radius. Since the size of the skyrmion is 1 nm for an atomic Fe layer on the Ir(111) surface [7], 3 nm for MnGe [8], 18 nm for MnSi [9], and 70 nm for FeGe [10], the corresponding emergent magnetic fields are $\sim$4000, 1100, 28, and 1 T, respectively.

This emergent magnetic field leads to the Hall effect [11]. Most of the studies focus on the Hall effect in metallic systems with large electron density [8,9,12,13]. This so-called topological Hall conductivity σ_{xy} is usually small compared with the longitudinal conductivity σ_{xx}, i.e., the Hall angle σ_{xy}/σ_{xx} is typically of the order of 10^{-2} at most [8].

Up to now, we regard skyrmions as the source of the real-space emergent magnetic field. When the size of the skyrmion becomes comparable to the mean free path, it is expected that the crossover from the real to momentum space Berry curvature occurs. In the latter case, there is no Landau-level (LL) formation, but the band structure is formed by taking into account the solid angle of the spin, and the intrinsic anomalous Hall effect appears whose conductance is given by the integral of the Berry curvature in momentum space [14,15]. A more drastic example is the quantized anomalous Hall effect (QAHE) in the magnetic topological insulator (TI), where the surface state with gap opening due to the exchange coupling to the magnetic ions produces the quantized Hall conductance of e^2/h without the external magnetic field [16].

It is expected that the SkX offers an ideal laboratory to study AHE from a unified viewpoint since one can change the size of the skyrmion, the mean free path, and even the carrier concentration by gating at the interface, to reveal the crossover between real and momentum Berry curvature and stability of the quantized Hall conductance as these conditions are changed.

In this paper we theoretically explore the emergence of the QAHE in the SkX without external magnetic field, which we call quantized topological Hall effect (QTHE). The band structure contains several well separated bands in the low electron-density regime, where each band has a Chern number $C = -1$. Consequently the emergence of the QTHE is predicted. We point out that the lowest and next-lowest bands are well described by the Dirac theory. On the other hand, Hall plateaux disappear in the large electron-density regime because of the overlap of bands. We also clarify the conditions of QTHE for the skyrmion size, carrier density, disorder strength, and temperature.

II. MODEL

We start with a free-electron system coupled with the background spin texture $\boldsymbol{n}_i$ by Hund's coupling [15,17,18]. The Hamiltonian is given by the double-exchange model,

$$H = \sum_{ij} t^{ij} c_i^\dagger c_j - J \sum \boldsymbol{n}_i c_i^\dagger \boldsymbol{\sigma} c_i, \tag{1}$$

where $c_i^\dagger$ (c_i) is the two-component (spin up and spin down) creation (annihilation) operator at the i site, t^{ij} is the transfer integral between nearest-neighbor sites, J is the Hund's coupling strength between the electron spin and background spin texture, and $\boldsymbol{\sigma}$ denotes the Pauli matrix. When Hund's coupling is strong enough $J \gg t^{ij}$, the spin of the hopping electron is forced to align parallel to the spin texture [15,18]. The wave function $|\chi(\boldsymbol{r})\rangle$ of the conduction electron at $\boldsymbol{r}$ corresponding to the localized spin $\boldsymbol{n}(\boldsymbol{r})$ is given by

$$|\chi(\boldsymbol{r})\rangle = \left(\cos\frac{\theta(\boldsymbol{r})}{2}, e^{i\phi(\boldsymbol{r})} \sin\frac{\theta(\boldsymbol{r})}{2} \right)^t, \tag{2}$$

where we have introduced the polar coordinate of the spin configuration $\boldsymbol{n} = (\cos\phi\sin\theta, \sin\phi\sin\theta, \cos\theta)$. Then the effective transfer integral is obtained:

$$t_{\rm eff}^{ij} = \cos\frac{\theta_i}{2}\cos\frac{\theta_j}{2} + \sin\frac{\theta_i}{2}\sin\frac{\theta_j}{2}e^{-i(\phi_i-\phi_j)} \tag{3}$$

$$= t\langle\chi_i|\chi_j\rangle = te^{ia_{ij}}\cos\frac{\theta_{ij}}{2}, \tag{4}$$

where

$$a_{ij} = \arctan\frac{-\sin(\phi_i-\phi_j)}{\cos(\phi_i-\phi_j)+\cot\frac{\theta_i}{2}\cot\frac{\theta_j}{2}} \tag{5}$$

is the vector potential generated by the spin between the i and j sites, and θ_{ij} is the angle between the two spins. The effective tight-binding Hamiltonian is obtained as

$$H = \sum_{ij} t_{\rm eff}^{ij} d_i^\dagger d_j, \tag{6}$$

where $d_i^\dagger$ (d_i) is the spinless creation (annihilation) operator at the i site. The detailed derivation is shown in the Appendix.

Skyrmion crystal

We consider a background spin texture $\boldsymbol{n}(\boldsymbol{r})$ made of a square SkX. Each skyrmion has a nontrivial topological number [19]. The skyrmion profile is well assumed as $\theta(\boldsymbol{r}) = \pi(1-r/\lambda)$ for $r < \lambda$ and $\theta(\boldsymbol{r}) = 0$ for $r > \lambda$. The emergent magnetic field is produced by the spin texture since it has a finite solid angle [1,20–22],

$$b_z(\boldsymbol{r}) = \frac{\hbar}{2e}\boldsymbol{n}\cdot(\partial_x\boldsymbol{n}\times\partial_y\boldsymbol{n}) = \frac{\hbar}{2e}\frac{\pi}{r\lambda}\sin\pi(1-r/\lambda) \tag{7}$$

for $r < \lambda$ and $b_z = 0$ for $r > \lambda$. It does not depend on the azimuthal angle ϕ. The total magnetic flux is

$$\int_0^\lambda d^2\boldsymbol{r}\, b_z(\boldsymbol{r}) = \Phi_0, \tag{8}$$

with $\Phi_0 = h/e$, and is independent of the skyrmion radius λ.

III. ELECTRONIC PROPERTIES

A. Band structure

The band structure can be obtained by numerically diagonalizing the effective Hamiltonian in the unit cell with the size $2\lambda \times 2\lambda$ in the presence of the SkX. The Brillouin zone is given by $-\pi/2\lambda < k_x, k_y < \pi/2\lambda$. Here we take the unit with the lattice constant $a = 1$. Then the unit cell has dimensionless area $(2\lambda)^2$. We show the band structure in the presence of SkX in Figs. 1(a) and 1(b), which are warped and the number of bands is $4\lambda^2$. There are finite gaps between two successive bands for lower bands. However, the band overlap starts at a higher band. In Fig. 1(c) shown the band structure of the corresponding uniform mean magnetic field. Here, since one skyrmion exists per area $4\lambda^2$, the mean magnetic field $\bar{b}$ is given by $\Phi_0/4\lambda^2$. It is seen that there is almost no energy dispersion, i.e., the Landau-level formation, with the energy separation Δ_0.

We show the gaps and overlaps of bands in Fig. 2(a) for various skyrmion radius λ, where the bands are marked in the color bar and the band gaps are denoted by the white blanks. We find that the band gap shows a scaling behavior for the skyrmion radius. The band gap between the lowest and second-lowest bands always opens.

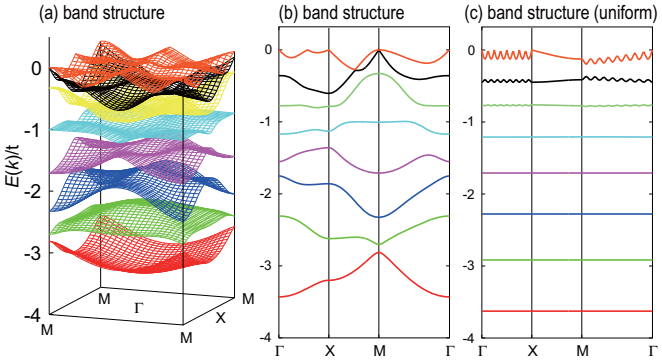

FIG. 1. (Color online) The band structure in the presence of SkX. We have set $\lambda = 2$. The horizontal axes are momentum k_x and k_y, while the vertical axis is the energy. There are $4\lambda^2 = 16$ bands. We show (a) a bird's eye view and (b) a cross section of the lowest eight bands. (c) The band structure of a tight-binding model with the uniform magnetic flux, which forms the almost flat Landau levels except near the center of the energy 0.

We show the λ dependence of the lowest band gap Δ in Fig. 2(b). It is proportional to $1/\lambda^2$. There is some deviation from the linear fit in small λ, which is probably due to the finite-size effect. We can compare this band gap with the Landau level separation Δ_0 shown in Fig. 1(c). The lowest Landau-level gap Δ_0 is given by 0.71t for $\lambda = 2$, while the lowest gap of the QTHE in SkX is given by $\Delta = 0.11$t. The linear relation in the small $1/4\lambda^2$ region of Fig. 2(b) indicates the relation $\Delta \cong \Delta_0/5$.

B. Berry curvature

We focus on the lowest and second-lowest bands [Fig. 3(a)]. We show the spin direction determined by $\langle\psi(\boldsymbol{k})|\sigma|\psi(\boldsymbol{k})\rangle$ for conduction and valence bands in Figs. 3(c) and 3(d), respectively, where the antivortex structure is evident at the M point. It implies that the spin texture has a nontrivial Berry curvature.

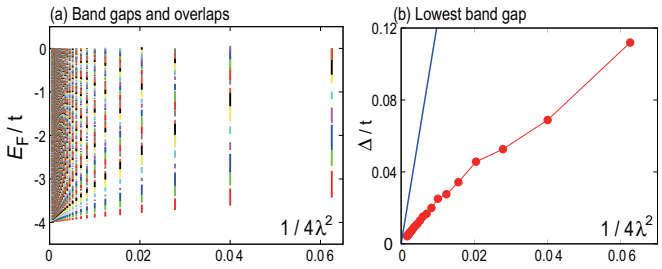

FIG. 2. (Color online) (a) Band gaps and overlaps for various sizes λ of the skyrmions. (b) The $(2\lambda)^{-2}$ dependence of the lowest band gap Δ. The gap is proportional to $(2\lambda)^{-2}$. The band gap of the system with the corresponding uniform mean magnetic flux is shown in the blue line.

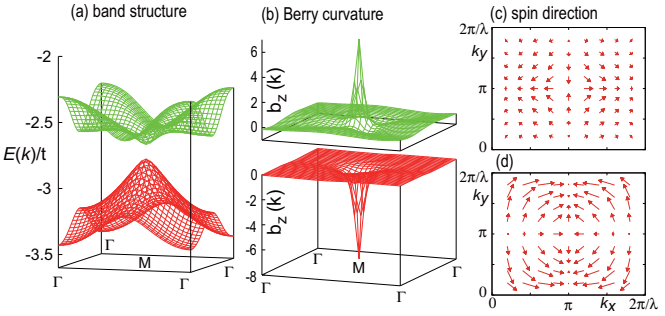

FIG. 3. (Color online) (a) Band structure of the lowest and second-lowest bands in the vicinity of the M point. It has the Dirac-cone shape. (b) The momentum distribution of the Berry curvature in the lowest and second-lowest bands. The Chern number consists of two parts: First, the Berry curvature takes the largest value at the M point, where the Chern numbers $C=-1/2$ and $+1/2$ are generated for these bands, respectively. Second, there are residual contributions to Chern numbers $C=-1/2$ and $-3/2$ away from the M point, and the total Chern number is an integer. Shown are the spin directions of the band structure of (c) the conduction and (d) valence bands. They clearly exhibit the antivortex structure at the M point.

We may define a "gauge potential" in the momentum space, $a_k(\boldsymbol{k})=-i\langle\psi(\boldsymbol{k})|\partial_k|\psi(\boldsymbol{k})\rangle$, for Bloch state $|\psi(\boldsymbol{k})\rangle$, which is properly called the Berry connection. Then we may define the "magnetic field" or the Berry curvature by $b_z(\boldsymbol{k})=\partial_{k_x}a_y(\boldsymbol{k})-\partial_{k_y}a_x(\boldsymbol{k})$. The Chern number is the integral of the Berry curvature over the first Brillouin zone, $\mathcal{C}=\frac{1}{2\pi}\int d^2k b_z(\boldsymbol{k})$.

We show the momentum dependence of the Berry curvature in Fig. 3. It takes a large value in the vicinity of the M point, which is $(k_x,k_y)=(\pi/2\lambda,\pi/2\lambda)$. The sign of the Berry curvatures are opposite between the lowest and second-lowest bands.

Each band has one unit Chern number $C=-1$, which is the same as that of Landau levels. One can consider an adiabatic pass from the uniform magnetic field to the space-dependent magnetic field induced by SkX. This deformation has no singularity.

The structure of the lowest and second-lowest bands has precisely the shape of the Dirac cone in the vicinity of the M point $(k_x,k_y)=(\pi/2\lambda,\pi/2\lambda)$ as in Fig. 3(a). This suggests that electrons are described by the Dirac theory $H=\hbar v(-k_x\sigma_x+k_y\sigma_y)+m\sigma_z$, where the mass m is related to the gap Δ between the lowest and second-lowest bands by $\Delta=2|m|$.

C. Edge states

The emergence of edge states is a strong signal indicating that the system is topological. It is called the bulk-edge correspondence. We have numerically diagonalized the Hamiltonian (6) in a nanoribbon geometry. The resultant band structure is shown in Fig. 4(a). The chiral edges are clearly observed between the two adjacent bands, which demonstrates a nonzero Chern number. More specifically, there are n chiral edge modes between the nth lowest and the $(n+1)$th lowest bands because the sum of the Chern numbers for the lowest n bands is n. In Fig. 4(b), we show the local density of states (DOS) of the edge state of the lowest band along the direction perpendicular to the nanoribbon direction. It is strictly localized at the outermost edge site, which is a strong signal of the topological edge states.

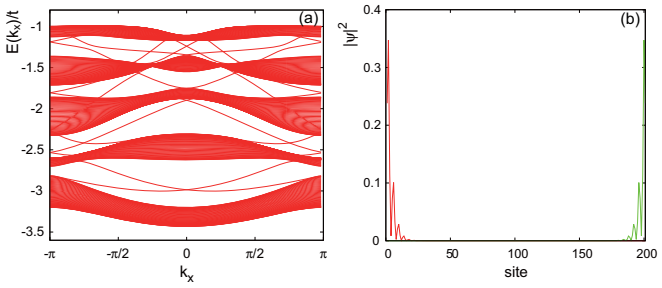

FIG. 4. (Color online) (a) The edge states of quantum topological Hall effects in a nanoribbon geometry. The chiral edges are clearly observed between the two adjacent bands, which demonstrates a nonzero Chern number. (b) The local DOS along the direction perpendicular to the nanoribbon direction. It is strictly localized at the outermost edge site, which is a strong signal of the topological edge state.

IV. HALL CONDUCTANCE

The conductance is calculated by the Kubo formula [23,24],

$$\sigma_{xy}=-\frac{ie^2}{h}\frac{2\pi}{L^2}\sum_{n,\boldsymbol{k}}f(E_{n\boldsymbol{k}})\times\sum_{m(\neq n)}\frac{\langle n\boldsymbol{k}|\frac{\partial H}{\partial k_x}|m\boldsymbol{k}\rangle\langle m\boldsymbol{k}|\frac{\partial H}{\partial k_y}|n\boldsymbol{k}\rangle-(n\leftrightarrow m)}{(E_{n\boldsymbol{k}}-E_{m\boldsymbol{k}})^2},\quad(9)$$

where n and m are the band indices and $f(x)$ is the Fermi distribution function. We show the Hall conductance in Fig. 5 calculated using the Kubo formula (9). At zero temperature, it is quantized to be the Chern number when the Fermi energy is inside the gap, $\sigma_{xy}=\frac{e^2}{h}\sum_{n:\text{filled}}C_n$, where C_n is the Chern number of the nth band. Below the band gap, the Hall conductance decreases, while it increases above the band gap. This is due to the fact that the sign of the Berry curvature

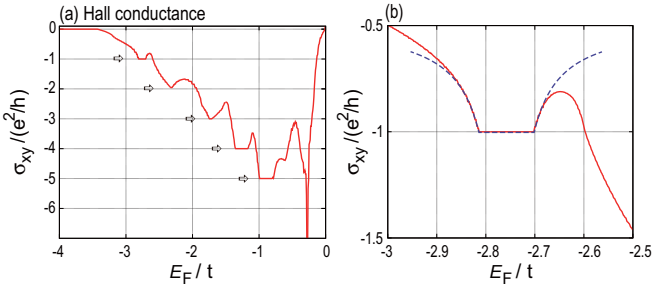

FIG. 5. (Color online) (a) The Hall conductance as a function of the chemical potential. The horizontal axis is the chemical potential, while the vertical axis is the Hall conductance σ_{xy}. The Hall conductance is quantized as marked by arrows. There is a peculiar structure of dips in the conductance at the values where it is quantized. (b) Zoom up of (a) near the band edge. It is well fitted by the dotted curve obtained in the Dirac theory.

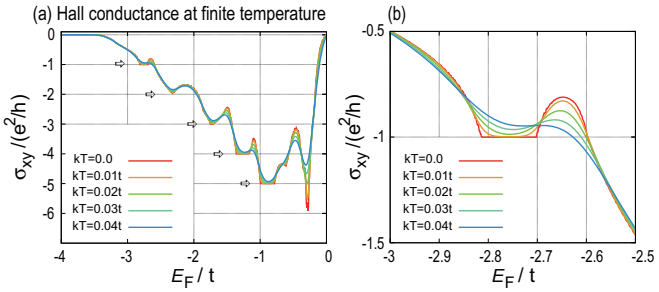

FIG. 6. (Color online) (a) The Hall conductance at finite temperature. Though it is not quantized, the peculiar dip structure is observable even at room temperature. (b) Zoom up of (a) near the band edge.

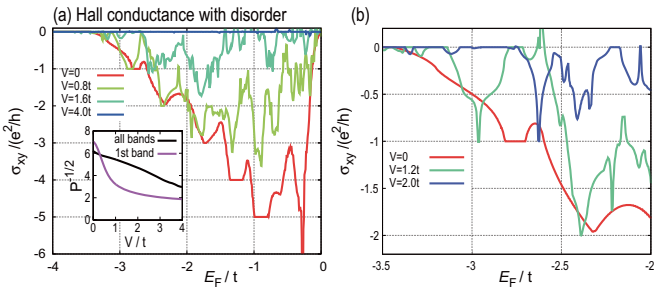

FIG. 7. (Color online) (a) The Hall conductance for various disorder strength. Disorder strength is indicated by the color. Hall plateaux disappear as disorder increases. However, the Hall plateau at $\sigma_{xy} = -e^2/h$ is reduced to be 0. (b) The Hall conductance in the vicinity of the band edge.

is opposite between the two adjacent bands. The total Chern number can be very large for large λ, which is distinct from the QAHE in magnetic topological insulators [16].

This behavior of the Hall conductance across the gap can be interpreted by the Dirac theory, which gives

$$\sigma_{xy} = \begin{cases} -1/2 & \text{for} \quad |\mu| < |m| \\ -m/(2|\mu|) & \text{for} \quad |\mu| > |m| \end{cases}. \tag{10}$$

It describes the peculiar behavior of the Hall conductance quite well as in Fig. 5(b), where the conductance is quantized inside the gap and continuously changes outside the gap showing a dip structure.

A. Finite temperature

We show the Hall conductance at finite temperature in Fig. 6. It is evident that the temperature scale is given by the gap Δ in Fig. 1(b), which is around $0.1t$ for $\lambda = 2$. Although the quantization of the plateau is broken at $k_B T = 0.01t \simeq 0.01$ eV $\simeq 100$ K, the peculiar dip structure toward the formation of the plateau is clearly visible even at $k_B T \simeq 400$ K. Consequently, our prediction of QTHE can be experimentally observable at room temperature.

B. Disorder effect

Up to now, we have focused on the pure system, and the Berry curvature in momentum space. Now we introduce the disorder potential as given by

$$H_{\text{imp}} = \sum_i U_i d_i^\dagger d_i, \tag{11}$$

where U_i takes a uniform random distribution for $-V < U_i < V$. We have calculated the Hall conductivity σ_{xy} for the system of size 8×8, including four unit cells. Figure 7 shows the numerical results, which clearly shows that the plateau transition occurs at $V \cong t$ for the lowest band, i.e., $\sigma_{xy} = -\frac{e^2}{h}$. Note that when $|\sigma| > \frac{1}{2}\frac{e^2}{h}$, the two-parameter scaling trajectory converges to the quantized Hall state. Taking this criterion, the lowest occupied band, which is the most promising candidate to observe the QTHE in SkX, can support the plateau up to $V \cong$ t. This magnitude of the random potential is similar to the separation between LLs in Fig. 1(c) and is much larger than the gap Δ in Fig. 1(b) which is $\cong 0.1t$ in the present case. This is because the dispersion gives the stability or robustness of the extended state. For higher energy bands, the Hall conductivity is reduced more slowly as V increases, and the criterion $|\sigma| > \frac{1}{2}\frac{e^2}{h}$ is satisfied up to $V \cong 3$t as shown in Fig. 7(a). We also calculated the quantity P_n for the eigenfunction $\langle i|\psi_n\rangle$ defined by

$$P_n = \sum_i |\langle i|\psi_n\rangle|^4, \tag{12}$$

which measures the extent of the wave function. Namely, when $\langle i|\psi_n\rangle$ extends over the M sites, $P_n \sim M^{-1}$. Therefore, the localization length is estimated by $P_n^{-1/2}$ in two dimensions. We show in the inset of Fig. 7 the averaged $P_n^{-1/2}$ for the lowest band (purple curve) and all the bands (black curve) as a function of V. It seen that the disappearance of the QTHE roughly corresponds to the localization of the wave functions less than 4, where 4 is the size of the unit cell (skyrmion). Therefore, since the mean free path ℓ is always longer than the localization length, the QTHE is observed only in the case where $\ell > 2\lambda$, i.e., the Berry curvature in momentum space is a more appropriate picture rather than that in the real space.

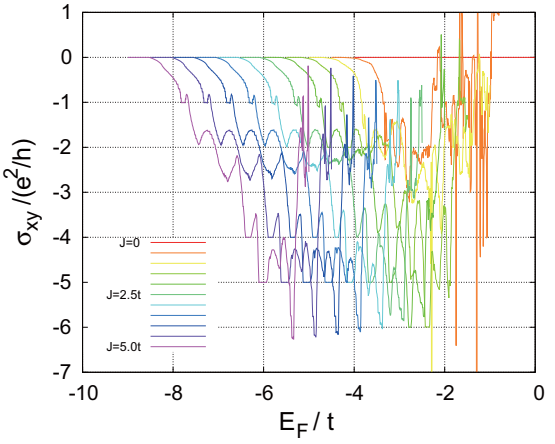

FIG. 8. (Color online) (a) The Hall conductance for various exchange coupling strength without assuming the strong exchange coupling limit. The Hall conductance is almost the same as that in the strong-coupling limit for $J > 3t$.

C. Finite exchange coupling

We have so far assumed the strong-coupling limit. However, this is not necessary for the quantization of the Hall conductance. In order to show this, we have explicitly diagonalized the Hamiltonian (1) with various values of exchange coupling J. The Hall conductance is displayed in Fig. 8, where the Hall plateaux are observed for $J > t$. For $J > 3t$, the Hall conductance is almost the same as that in the strong-coupling limit in Fig. 5. This result shows that the results obtained in the strong-coupling limit are actually valid for a wide range of parameters.

V. DISCUSSION

The electron density should be of the order of one electron per skyrmion, whose electron density is given by $1/4\lambda^2$. In order to realize experimental situations, it is necessary to reduce the number of electrons. For the skyrmion size λ ranging from $\lambda \sim 1$ nm to $\lambda \sim 100$ nm, the corresponding electron density n is from $n \sim 10^{14}$ cm^{-2} to $n \sim 10^{10}$ cm^{-2}. In this sense, an interface of dilute magnetic semiconductors MnGaAs/AlGaAs will be promising [25]. The sheet carrier density of Mn doped GaAs is about 10^{12} cm^{-2}. The interface of $LaAlO_3/SrTiO_3$ (LAO/STO) is another candidate where a ferromagnetic metal is realized [26,27]. The carrier density of an interface of LAO/STO is about 10^{13} cm^{-2}. The broken inversion symmetry at these interfaces induces the Rashba interaction and stabilizes the skyrmion crystal. Furthermore, by applying gate voltage with the use of the electric-double-layer-transistor (EDLT) technique, it is possible to modulate the chemical potential to the order of some eV, which enables us to control the carrier density widely. At the same time, in the Rashba system such as interfaces, the amplitude of the Rashba coupling can be enhanced, which implies that one can reduce the size of skyrmion and furthermore enlarge the gap size, which is proportional to $1/\lambda^2$. These two kinds of modulation, i.e., the chemical potential and the skyrmion size, allow us to tune the chemical potential to be inside the gap.

The QTHE is robust against disorder as in the case of system with corresponding uniform magnetic field with Landau levels. Considering the very large mean magnetic field of ~4000 T for the skrmion size $\lambda \sim 1$ nm, the disorder does not destroy the QTHE so seriously. This is because the change in the Chern numbers occurs only via the pair annihilation, and the appreciable energy dispersion of the band in SkX protects the Chern number. On the other hand, the band gap Δ of SkX is smaller than Δ_0, i.e., that of the corresponding system with uniform magnetic field, and hence the stability against the thermal excitation is reduced. Δ is estimated as $\Delta_0/5$ but, as mentioned above, the emergent magnetic flux induced by SkX is gigantic and the QTHE even at room temperature is expected.

Note added. There are some proposals on QAHE with magnetic texture. Graphene proximity coupled to an antiferromagnet insulator is an example [28], where the gap is given by 7 meV. Another example, which appeared after the submission of present work, is graphene proximity coupled to skymions [29], where the gap is of the order of 30 meV. The advantage of our model is that the gap is of the order of 100 meV, which is higher than those presented in these works.

ACKNOWLEDGMENTS

This work was supported in part by JSPS KAKENHI Grants No. 24224009, No. 25400317, No. 15H05854, and No. 26103006.

APPENDIX: DERIVATION OF THE EFFECTIVE HAMILTONIAN

The Hamiltonian is given by the double-exchange model,

$$H = \sum_{ij} t^{ij} c_i^\dagger c_j - J \sum \boldsymbol{n}_i c_i^\dagger \boldsymbol{\sigma} c_i, \tag{A1}$$

where $c_i^\dagger$ (c_i) is the two-component (spin up and spin down) creation (annihilation) operator at the i site, t^{ij} is the transfer integral between nearest-neighbor sites, J is the Hund's coupling strength between the electron spin and the background spin texture, and $\boldsymbol{\sigma}$ denotes the Pauli matrix. When Hund's coupling is strong enough, $J \gg t^{ij}$, the spin of the hopping electron is forced to align parallel to the spin texture [18].

We diagonalize the Hund's coupling term so that the spin direction is always up,

$$U_i^\dagger (\boldsymbol{n} \cdot \boldsymbol{\sigma}) U_i = \sigma_z. \tag{A2}$$

It can be diagonalized by setting

$$U_i^\dagger = \boldsymbol{m}_i \cdot \boldsymbol{\sigma} \tag{A3}$$

with

$$\boldsymbol{m} = \left(\sin\frac{\theta}{2}\cos\phi, \sin\frac{\theta}{2}\sin\phi, \cos\frac{\theta}{2} \right). \tag{A4}$$

The electron operator is transformed by this gauge transformation as

$$c_i = U_i d_i. \tag{A5}$$

In the new electron operator d_i, the Hamiltonian reads

$$H = \sum_{ij} t^{ij} d_i^\dagger U_i^\dagger U_j d_j - J \sum d_i^\dagger \sigma_z d_i. \tag{A6}$$

Then the effective hopping is given by

$$t_{\text{eff}}^{ij} = t^{ij} U_i^\dagger U_j, \tag{A7}$$

which is calculated as

$$U_i^\dagger U_j = \begin{pmatrix} \cos\frac{\theta_i}{2}\cos\frac{\theta_j}{2} + \sin\frac{\theta_i}{2}\sin\frac{\theta_j}{2} e^{-i(\phi_i-\phi_j)} & -e^{i\phi_i}\sin\frac{\theta_1}{2}\cos\frac{\theta_j}{2} + e^{-i\phi_j}\cos\frac{\theta_i}{2}\sin\frac{\theta_j}{2} \\ e^{-i\phi_i}\sin\frac{\theta_i}{2}\cos\frac{\theta_j}{2} e^{i\phi_j} \cos\frac{\theta_i}{2}\sin\frac{\theta_j}{2} & \cos\frac{\theta_i}{2}\cos\frac{\theta_j}{2} + \sin\frac{\theta_i}{2}\sin\frac{\theta_j}{2} e^{i(\phi_i-\phi_j)} \end{pmatrix}. \tag{A8}$$

For the strong-coupling limit only the component that is parallel to the spin direction is active,

$$t_{\mathrm{eff}}^{ij} = \cos\frac{\theta_i}{2}\cos\frac{\theta_j}{2} + \sin\frac{\theta_i}{2}\sin\frac{\theta_j}{2}e^{-i(\phi_i-\phi_j)}. \tag{A9}$$

The absolute value of the effective transfer integral is given by

$$\left|t_{\mathrm{eff}}^{ij}\right|^2 = \frac{1+\cos\theta_i\cos\theta_j+\cos(\phi_i-\phi_j)\sin\theta_i\sin\theta_j}{2} \tag{A10}$$

$$= \frac{1+\cos\theta_{ij}}{2} = \cos^2\frac{\theta_{ij}}{2}, \tag{A11}$$

where θ_{ij} is the angle between the two spins,

$$\cos\theta_{ij} = \boldsymbol{m}_i\cdot\boldsymbol{m}_j = \cos\theta_i\cos\theta_j+\cos(\phi_i-\phi_j)\sin\theta_i\sin\theta_j. \tag{A12}$$

The effective transfer integral is written as

$$t_{\mathrm{eff}}^{ij} = e^{ia_{ij}}\cos\frac{\theta_{ij}}{2} \tag{A13}$$

with the vector potential

$$a_{ij} = \arctan\frac{-\sin(\phi_i-\phi_j)}{\cos(\phi_i-\phi_j)+\cot\frac{\theta_i}{2}\cot\frac{\theta_j}{2}}. \tag{A14}$$

[1] N. Nagaosa and Y. Tokura, Nat. Nanotechnol. **8**, 899 (2013).
[2] N. Bogdanov and D. A. Yablonskii, JETP **68**, 101 (1989).
[3] N. Bogdanov and A. Hubert, J. Magn. Magn. Mater. **138**, 255 (1994).
[4] U. K. Roessler, N. Bogdanov, and C. Pfleiderer, Nature (London) **442**, 797 (2006).
[5] S. Mühlbauer, B. Binz, F. Jonietz, C. Pfleiderer, A. Rosch, A. Neubauer, R. Georgii, and P. Böni, Science **323**, 915 (2009).
[6] X. Z. Yu, Y. Onose, N. Kanazawa, J. H. Park, J. H. Han, Y. Matsui, N. Nagaosa, and Y. Tokura, Nature (London) **465**, 901 (2010).
[7] S. Heinze, K. von Bergmann, M. Menzel, J. Brede, A. Kubetzka, R. Wiesendanger, G. Bihlmayer, and S. Blügel, Nat. Phys. **7**, 713 (2011).
[8] N. Kanazawa, Y. Onose, T. Arima, D. Okuyama, K. Ohoyama, S. Wakimoto, K. Kakurai, S. Ishiwata, and Y. Tokura, Phys. Rev. Lett. **106**, 156603 (2011).
[9] M. Lee, W. Kang, Y. Onose, Y. Tokura, and N. P. Ong, Phys. Rev. Lett. **102**, 186601 (2009).
[10] X. Z. Yu, N. Kanazawa, Y. Onose, K. Kimoto, W. Z. Zhang, S. Ishiwata, Y. Matsui, and Y. Tokura, Nat. Mater. **10**, 106 (2011)
[11] T. Schulz, R. Ritz, A. Bauer, M. Halder, M. Wagner, C. Franz, C. Pfleiderer, K. Everschor, M. Garst, and A. Rosch, Nat. Phys. **8**, 301 (2012).
[12] Y. Li, N. Kanazawa, X. Z. Yu, A. Tsukazaki, M. Kawasaki, M. Ichikawa, X. F. Jin, F. Kagawa, and Y. Tokura, Phys. Rev. Lett. **110**, 117202 (2013).
[13] A. Neubauer, C. Pfleiderer, B. Binz, A. Rosch, R. Ritz, P. G. Niklowitz, and P. Böni, Phys. Rev. Lett. **102**, 186602 (2009).
[14] Y. Taguchi, Y. Oohara, H. Yoshizawa, N. Nagaosa, and Y. Tokura, Science **291**, 2573 (2001).
[15] M. Onoda, G. Tatara, and N. Nagaosa, J. Phys. Soc. Jpn. **73**, 2624 (2004).
[16] C.-Z. Chang *et al.*, Science **340**, 167 (2013).
[17] P. W. Anderson and H. Hasegawa, Phys. Rev. **100**, 675 (1955).
[18] K. Ohgushi, S. Murakami, and N. Nagaosa, Phys. Rev. B **62**, 6065(R) (2000).
[19] R. Rajaraman, *Solitons and Instantons* (Elsevier, New York, 1987).
[20] G. Volovik, J. Phys. C **20**, L83 (1987).
[21] S. Zhang and Steven S.-L. Zhang, Phys. Rev. Lett. **102**, 086601 (2009).
[22] J. Zang, M. Mostovoy, J. H. Han, and N. Nagaosa, Phys. Rev. Lett. **107**, 136804 (2011).
[23] D. J. Thouless, M. Kohmoto, M. P. Nightingale, and M. den Nijs, Phys. Rev. Lett. **49**, 405 (1982)
[24] M. Kohmoto, Ann. Phys. (NY) **160**, 343 (1985).
[25] A. M. Nazmul, S. Sugahara, and M. Tanaka, Phys. Rev. B **67**, 241308(R) (2003).
[26] A. D. Caviglia, S. Gariglio, N. Reyren, D. Jaccard, T. Schneider, M. Gabay, S. Thiel, G. Hammerl, J. Mannhart, and J.-M. Triscone, Nature (London) **456**, 624 (2008).
[27] C. Bell, S. Harashima, Y. Kozuka, M. Kim, B. G. Kim, Y. Hikita, and H. Y. Hwang, Phys. Rev. Lett. **103**, 226802 (2009).
[28] Z. Qiao, W. Ren, H. Chen, L. Bellaiche, Z. Zhang, A. H. MacDonald, and Q. Niu, Phys. Rev. Lett. **112**, 116404 (2014).
[29] J. L. Lado and J. Fernandez-Rossier, arXiv:1505.00732.